A variational framework for distortion correction, segmentation and cortical parcellation of diffusion MRI

Oscar Esteban*, *Member, IEEE*, Alessandro Daducci, *Member, IEEE*, Meritxell Bach-Cuadra, *Member, IEEE*, Jean-Philippe Thiran, *Member, IEEE*, Andrés Santos, *Member, IEEE*, and Dominique Zosso, *Life Fellow, IEEE*

Fix Memberships

Abstract-In whole-brain connectivity analysis of diffusion MRI (dMRI) data, an accurate delineation of the white-matter and grey-matter interfaces is required. While high-standard segmentation is readily available for structural MRI, dMRI typically present significant cerebrospinal fluid contamination effects, mainly derived from its typical low resolution, and severe geometrical distortions. We propose a segmentation-registration variational framework that exploits the detailed anatomy extracted from structural MRI as shape-prior. We use an "active contours without edges"-like model to search for a deformation field that optimally maps the shape prior on multivariate dMRIderived data in diffusion space, registering structural and diffusion coordinate spaces and implicitly segmenting dMRI data. The approach proven the intrinsic coupling of segmentation and distortion correction and we evaluate its results on a digital simulated phantom and real datasets. Therefore, precise and consistent cortical parcellation on dMRI is straightforward by projection from T1 space, avoiding additional registration, segmentation and/or surface matching steps.

Index Terms—diffusion MRI, susceptibility distortion, segmentation, registration, parcellation, shape-prior.

I. INTRODUCTION

DIFFUSION magnetic resonance imaging (MRI) is a widely used family of MRI techniques [1] which accounts for a growing interest in its application to structural connectivity analyses of the brain at the macro-scale [2]. This

Manuscript received XXX XX, 2013; revised XXX XX, 2013. This study is supported by: the Spain's Ministry of Science and Innovation (projects TEC2010-21619- C04-03, TEC2011-28972-C02-02, CDTI-CENIT AMIT and INNPACTO PRECISION), Comunidad de Madrid (ARTEMIS) and European Regional Development Funds; the Center for Biomedical Imaging (CIBM) of the Geneva and Lausanne Universities and the EPFL, as well as the Leenaards and Louis Jeantet foundations. *Asterisk indicates corresponding author*.

*O. Esteban is with the Biomedical Image Technologies (BIT), ETSI Telecomunicación, Universidad Politécnica de Madrid and CIBER-BBN, Madrid, Spain, and the Signal Processing Laboratory (LTS5), École Polytechnique Fédérale de Lausanne (EPFL), Lausanne, Switzerland (e-mail: phd@oscaresteban.es).

A. Daducci is with the Signal Processing Laboratory (LTS5), École Polytechnique Fédérale de Lausanne (EPFL), Lausanne, Switzerland.

M. Bach-Cuadra and JP. Thiran are with the Signal Processing Laboratory (LTS5), École Polytechnique Fédérale de Lausanne (EPFL), Lausanne, Switzerland, and Dept. of Radiology, University Hospital Center (CHUV) and University of Lausanne (UNIL), Lausanne, Switzerland.

A. Santos is with the Biomedical Image Technologies (BIT), ETSI Telecomunicación, Universidad Politécnica de Madrid and CIBER-BBN, Madrid, Spain.

D. Zosso is with the Department of Mathematics, University of California, Los Angeles (UCLA), Los Angeles, CA, US and is supported by the Swiss National Science Foundation (SNF) under grant PBELP2-137727.

emerging field exploits diffusion MRI (dMRI) data to derive the local axonal structure at each imaging voxel [3] and estimate a whole-brain mapping of fiber tracts [4, 5] represented by trajectories reconstructed from the local information. This comprehensive map of neural connections of the brain is called the *connectome* [6, 7]. The connectome analysis is a promising tool for neuroscience [8] and for the clinical application [9] as well.

Early dMRI research mainly focused on the improvements of imaging methodologies by a better understanding of the diffusion effect, and improving image reconstruction methodologies. Currently, the connectome extraction and analysis relies on a large chain of sophisticated computational techniques including acquisition, reconstruction, modeling and model fitting, image segmentation and registration, fibre tracking, connectivity mapping, visualization, statistical group studies, and inference [10]. This growing complexity has given rise to challenging issues towards reliable structural information about the neuronal tracts presented in, and also difficulties on the statistical analysis [11, 12]. To our knowledge, studies regarding the impact of the different sources of inaccuracy and variability along the toolchain for connectivity analysis [13– 15] are scarce. Here, we shall address three tasks included within the image processing stage in a unified approach: brain tissue segmentation in diffusion space (subsection I-B), correction of geometrical distortions (subsection I-C), and structural image registration to diffusion coordinate space (subsection I-D). These tasks are generally solved independently, or combined in pairs. However, there exist fundamental coupling relationships that can be exploited to obtain a simultaneous solution to the three problems. This joint approach satisfactory impacts the downstream outcomes of the whole pipeline with the increase of the internal consistency.

A. DMRI data overview

dMRI data are usually acquired with echo-planar imaging (EPI) sequences as they allow for very fast acquisition of large sets of slices each acquired after a single excitation [16, 17]. EPI volumes are collected in sequence and each one represents one probed diffusion direction. This first acquisition is called *raw* data or *diffusion signal*. One or more volumes without directional encoding (so-called *baseline*, b=0, *low b*, or just B0 volumes) are interleaved as reference, at the least one is acquired at the beginning of the EPI dataset. These

EPI are known to suffer from geometrical distortions and artifacts due to, mainly, three sources: the subject motion in between acquiring different sampling directions, the induced *eddy currents* on the scanner coils due to the gradient switching [18], and, finally, distortions caused by the magnetic susceptibility inhomogeneity present at tissue interface. *Susceptibility distortions* happen along the phase-encoding direction, and are most appreciable in the frontal part of the brain due to the air/tissue interface located around the sinuses. Two implications are associated to this artifact: the signal loss caused on highly distorted regions, and a significant added difficulty in registering with structural images (e.g. T1-weighted).

After correcting for artifacts, the difficulty of performing analyses directly on the *directionally dependent* raw data is not affordable. Thus, dMRI data is reconstructed using one of a numerous set of readily available algorithms. The outcome is a voxel-wise model of diffusion shape (in [19] there is available a comprehensive review of state-of-art methodologies). On top of the chosen model, some scalar maps describing tissue features is generally computed. For instance, the most popular dMRI-derived scalar map is fractional anisotropy (FA) which depicts the isotropy of water diffusion inside the brain. Another widely studied map is the apparent diffusion coefficient (ADC) (or mean diffusivity (MD) that has a dual definition), which reflects the intensity of the diffusion effect. Many other directionally invariant measurements have been defined. For a comprehensive study, we refer to [20].

Alongside distortions and direction dependency, dMRI data is strongly affected by partial volume effects (PVEs) [21] that appears when several different tissues, or signal emitters, are present in the same imaging unit, producing an averaged intensity. The effect is directly related to the low resolution achievable with dMRI (typically around $2.0 \times 2.0 \times 2.0 mm^3$). An additional complication specific to dMRI is the cerebrospinal fluid (CSF) *contamination* [22], that is a particular PVE in which the signal sensed inside the affected voxel is linear with respect the grey matter (GM) and white matter (WM) contributions, but non-linear with respect CSF.

B. DMRI segmentation

A precise delineation of the CSF, GM and WM interfacing surfaces is required with sub-pixel resolution, because whereas tractography algorithms are very good at estimating the location of bundles in deep WM, they are not god (yet) at identifying where the tracts project into the GM (limitations on the termination criteria, [2, 23]). Thus, a WM segmentation is required by most of the available tractography algorithms to *filter* the resulting tractogram. The GM-WM interface is necessary to locate the starting and ending points of the detected fiber bundles, and CSF-WM surface is critical for pruning spurious and discontinued fiber bundles.

A number of methodologies have been proposed for dMRI segmentation, ranging from intensity thresholding to atlasbased segmentation. The first approach is performed simply

thresholding the FA map. Although this methodology was popular among the pioneer tractography studies, they were generally limited to certain regions or significant fiber tracts, and thus, it cannot be applied in whole-brain tractography. Early approaches to dMRI segmentation include level set formulations using scalar maps of direction invariants derived from the tensor model [24], directly on the diffusion raw data [25], or finding alternative diffusion representations [26]. Even though this latter case was restricted to the extraction of the corpus callosum from a real dataset, the density of the components of the diffusion tensor are approximated by multivariate Gaussians for first. Iterative clustering performed on the B0 volumes of dMRI data was proposed by [27]. Later studies investigated the application of probabilistic frameworks combining mixtures of gaussians, Markov Random Field (MRF) and labeling fusion techniques [28] using as features widely-used dMRI-derived scalar maps as FA or MD. A similar framework combining co-registered structural information (T1 weighted) with independent orthogonal invariants derived from the dMRI tensor model was proposed by [29]. Some proposals suggest the use of the raw diffusion data (directionally dependent) to avoid fitting a certain model [30]. In [31], graph-cuts voxel-based techniques are proposed using the most common diffusion tensor derived features. Further developments of the probabilistic approach have been proposed adding more scalar maps as features and a more detailed treatment of PVE [32].

A number of methods have been proposed using features not directly derived from dMRI data. Segmentation obtained by co-registering structural T1-weighted images will be covered in subsection I-D.

None of the presented methods have claimed for definite results, mainly due to the lack of a *gold-standard* evaluation methodology. Most of them are tested only on certain regions, or do not provide sub-pixel resolution results [27–31]. Generally, results obtained with high resolution atlas co-registration (subsection I-D) are more compelling, limiting the activity on dMRI segmentation. However, recently [33] proposed to include this task within reconstruction algorithms. Finally, some *golden*-standard evaluation frameworks for task-based validation have been proposed for the segmentation results (e.g. lesion detection in visceral organs [34]).

reference to a summary table

C. Correction for susceptibility distortions

One approach to correcting the susceptibility distortions was proposed with the earliest EPI sequences used in functional MRI, and relies on the acquisition of extra MRI data. Generally, a gradient echo sequence (GRE) is used to obtain a map of magnitude and phase of the actual magnetic field inside the scanner. Based on this *fieldmap* and the theory underlying the distortion, [35] proposed a correction methodology. A number of forked and improved methodologies have been developed to correct for the susceptibility distortion and received the generic name of "fieldmap correction" techniques [36, 37].

Some other retrospective methodologies do not make use of the fieldmaps, as explicitly modeling the distortion [38],



registering with (anatomically correct) T2-weighted MRI [39–42] (we shall cover these methods in subsection I-D), or acquiring an extra B0 image with reversed phase encoding direction [43, 44].

A comparison of the diverse correction techniques is found in [45]. This study claims that fieldmap correction methodologies are not entirely accurate and reliable, even though the method is correct in principle. The conclusion was later confirmed by [42]. Additional concerns regarding fieldmap correction are the requirement of an extra acquisition (that is not always met or it is impractical), or the accuracy of the measured fieldmap that is sensitive to various effects (such us respiration, blood flow, etc.). All these factors have turned susceptibility distortion in EPI sequences an active field of research for the last 10 years.

D. Structural information co-registration

The last addressed task in the image processing stage of the studied connectivity analysis pipelines is the structural information co-registration. The need for this registration step is mainly raised when defining the nodes of the connectivity matrix. This definition step is named cortical parcellation as it imposes the regions that will be considered to cluster the fiber bundles reaching the WM-GM surface. The common procedure to accomplish this clustering is using a predefined parcellation in a high-resolution structural T1-weighted atlas (e.g. [46]). The second goal that has justified the applicability of structural images co-registration is susceptibility distortion correction as presented in subsection I-C. In any case, susceptibility distortion hinders a rigid-registration solution to this problem. Additionally, when applying non-linear intensitybased registration algorithms, other difficulties have to be addressed as the significant PVE in the WM-GM layer, or the inherent inadequacy of the B0 contrast (the only directionally *independent* existing in the raw dMRI data) due to the almost null difference in intensity between WM and GM pixels. Early registration methods appeared targeting the distortion correction. They quickly standardized the choice of T2 as anatomically correct source to be registered against the B0 in dMRI. B0 images have a very similar contrast to T2 weighted due to the parallelism of acquisition sequences. However, parcellation is defined in T1 weighted space, adding an additional registration step is generally overlooked by existing literature. Even though this processing stage has a very low complexity compared to the remaining tasks of the pipeline process, it is one additional source of inconsistency and unreliability.

One of the first proposals is [39], where the deformation field is modeled with B-Splines, the cost function is least squares and optimized in a multi-resolution gradient descent strategy. Their method is evaluated in both synthetic and real 2D images. Similarly, [40] proposed a spline-based deformation but including a weighting factor proportional to the Jacobian of the transform to correct the intensity of the undistorted data. They also use the log of the signal to enhance the low-signal regions, and optimize with a gradient descent algorithm the mutual information of the mapping. This framework set the basis for the following works. For instance, [45] also proposed

a B-Spline registration providing quantitative comparisons with fieldmap correction methods. Recent approaches take into account the signal loss due to dephasing [41], or introduce more complex variational frameworks [42].

The significant benefits of exploiting the anatomical MRI when segmenting the dMRI data have been demonstrated [47], justifying the use of the shape prior information. To our knowledge, there is no study simultaneously taking advantage from segmentation or distortion correction tasks to be applied to the co-registration problem.

E. Summary

All the available dMRI-derived models and scalar maps are very sensitive to distortions, PVE, noise and axonal dispersion [23], what yields numerous challenges in the processing tasks (artifact correction, segmentation, registration and parcellation). Finally, as a result a vast number of challenges and pitfalls emerge regarding accuracy (correctness) and precision (reproducibility) of tractography-based analyses [15] and connectome analyses.

Moreover, the problems of precise segmentation in dMRI-space and the spatial mapping between these contours and the corresponding surfaces in anatomical images bear significant redundancy. Once the spatial relationship between T1-weighted (T1) and dMRI space is established, the contours which are readily available in T1 space can simply be projected on to the dMRI data. Conversely, if a precise delineation in dMRI space was achieved, the spatial mapping with T1-space could be derived from one-to-one correspondences on the contours. However, neither segmentation nor registration can be performed flawlessly, if considered independently.

In this paper we propose a novel registration framework to simultaneously solving the segmentation, distortion and cortical parcellation challenges, by exploiting as strong shapeprior the detailed morphology extracted from high-resolution and anatomically correct MRI. Indeed, hereafter we assume this segmentation problem in anatomical images is reliably and accurately solved with readily available tools (e.g. [48]). After global alignment with T1 using existing approaches, the remaining spatial mismatch between anatomical and diffusion space is due to susceptibility distortions. Finally, we need to establish precise spatial correspondence between the surfaces in both spaces, including the tangential direction for parcellation. Therefore, we can reduce the problem to finding the differences of spatial distortion in between anatomical and dMRI space. We thus reformulate the segmentation problem as an inverse problem, where we seek for an underlying deformation field (the distortion) mapping from the structural space into the diffusion space, such that the structural contours segment optimally the dMRI data. In the process, the one-toone correspondence between the contours in both spaces is guaranteed, and projection of parcellisation to dMRI space is implicit and consistent.

We test our proposed joint segmentation-registration model on two different synthetic examples. The first example is a scalar sulcus model, where the CSF-GM boundary particularly suffers from PVE and can only be segmented correctly thanks to the shape prior and its coupling with the inner, GM-WM boundary through the imposed deformation field regularity. The second case deals with more realistic dMRI data stemming from phantom simulations of a simplistic brain data. Again, we show that the proposed model successfully segments the dMRI data based on two derived scalar features, namely FA and MD, while establishing an estimate of the dense distortion field.

The rest of this paper is organized as follows. First, in section II we introduce our proposed model for joint multivariate segmentation-registration. Then we provide a more detailed description of the data and experimental setup in section III. We present results in section IV and conclude in section V.

II. METHODS

A. Related work

Active contours without edges (ACWE) and level-set based formulations have been widely applied in image processing, as reviewed in [49]. We suggest clustering the current methodologies of template-based segmentation methods into three groups. The first group typically adds a shape prior term to the energy functional of an evolving active contour [50-54]. These methods generally have an explicit description of the expected relative boundary locations of the object to be delineated, and some even model the statistical deviations from this average shape. By including a coordinates mapping, it is possible to perform active contours based registration between timesteps in a time-series or between different images [55–59]. A summary of these second set of techniques is performed in [60], proposing two different approaches to applying the Mumford-Shah [61] functional in joint registration and segmentation. Finally, a derivation of the latter groups is composed by atlas-based segmentation methods [62–66], where the prior imposes consistent voxel-based classification of contiguous regions. A comprehensive summary of the ACWE-derived methodologies with special attention to joint registration-segmentation methods is found in [63].

Our joint registration and segmentation method is mainly inspired in the active deformation fields presented by [63], that is a generalization of the methodologies under second and third groups before. As it is described in their work, the first joint "morphing"-segmentation approach (it was not a proper registration method) was proposed in [55]. The first registration framework is presented by [67] where the energy functional is defined simultaneously in the moving and target images with an affine transformation supporting the coordinates mapping ("2 PDEs approach"). [58] proposed the first atlas-based registration based on the level set framework and using only one PDE. [68] extended the idea of [55, 67] for non-linear registration with a dense deformation field as mapping function. [60] combining ideas from both branches and proposed the propagation of the deformation field from the contours to the whole image definition. Finally, [63] present a comprehensive generalization of the methodologies.

All the surveyed frameworks are deduced from the general level set evolution equation introduced by [69]:

$$\frac{\partial \Phi_D(\mathbf{x}, t)}{\partial t} = \nu(\Phi_D(\mathbf{x}, t)) |\nabla \Phi_D(\mathbf{x}, t)|$$
(1)

where ν is the velocity of the flow or speed function that contains the local segmentation and contour regularization constraints, and $\Phi_D:\Omega\to\mathbb{R}$ is the signed distance function often used to represent implicitly the active contour by its zero level. An early extension to image registration was proposed by [58] but replacing Φ_D by the intensity function of the image to register, $\Phi_I:\Omega\to\mathbb{R}$ (the moving image). [55, 58] then define the speed function as $\nu(\Phi_I(\mathbf{x},t))=\Phi_I(\mathbf{x},t)-\Phi_T(\mathbf{x},t)$, where $\Phi_T(\mathbf{x})$ is the intensity function of the target image. Finally, [63] propose a different multiphase label function as level set function (Φ_L) that improves registration results.

Naming Φ_G a generic objective function, a dense deformation field of vectors $u: \mathbb{R}^n \to \mathbb{R}^n$ (tipically $n=\{2,3\}$) is introduced. Then, the conservation of the morphological description is assumed, such as $\Phi_G(\mathbf{x},t) = \Phi_G(\mathbf{x}+du,t+dt) \implies d\Phi_G(\mathbf{x},t) = 0$, where $d\Phi_G$ is the total derivative of Φ_G . Using the chain rule, it can be rewritten as the evolution equation of a vector flow:

$$\frac{\partial u(\mathbf{x},t)}{\partial t} = -\frac{\Phi_G}{|\nabla \Phi_G|} N_{\Phi_G},\tag{2}$$

where N_{Φ_G} is the normal of the level set. Finally, they introduce the general level set evolution equation into the vector flow to perform the registration task:

$$\frac{\partial u(\mathbf{x},t)}{\partial t} = -\nu(\Phi_G(\mathbf{x},t))N_{\Phi_G}.$$
 (3)

Therefore, the position of the level set function Φ_G at time t is given by the deformation field $u(\mathbf{x},t)$ and the initial level set function $\Phi_G(\mathbf{x},0)$, yielding:

$$\frac{\partial u(\mathbf{x},t)}{\partial t} = -\nu(\Phi_G(\mathbf{x} + u(\mathbf{x},t),0))N_{\Phi_G}.$$
 (4)

Here, we propose an active deformation field framework with some differences in the formulation of the problem. The main diverging points with respect to [63] are: 1) there is no need for an explicit level set function Φ_G , as we replace the level set gradient computation N_{Φ_G} with shape gradients [70, 71]; 2)

regularization is also based on linear diffusion smoothing REF-thirion, but they use a Gaussian filtering)

; 3) optimization is applied in the spectral domain, observing anisotropic and inhomogeneous mappings along each direction.

B. Bridging segmentation frameworks

A widely used approach to image segmentation is derived from the Bayes' rule (5). This framework seeks for a partitioning of a certain observation of features $F: \mathbb{R}^n \to \mathbb{R}^C$ (an *n*-dimensional *image* comprising C different channels) in piecewise smooth regions $\Omega = \{\Omega_l, l \in [1...L]\}$, that maximize the *a posteriori* probability $p(\Omega \mid F)$:

$$p(\Omega \mid F) = \frac{p(F \mid \Omega) p(\Omega)}{p(F)},$$
 (5)

where $p(F \mid \Omega)$ is the *likelihood* of the realization of F given a certain region set Ω . The second term, $p(\Omega)$, is the a-priori probability of the partitioning. Finally, p(F) is the

probability of a certain image realization, and thus, it will remain constant when computing the maximum a posteriori (MAP). Consequently, the Bayes' rule can be simplified for the optimization as follows:

$$p(\Omega \mid F) \propto p(F \mid \Omega) p(\Omega).$$
 (6)

In the simplest Bayesian segmentation framework, the unknown is the parameter set Θ_l of region-wise descriptors that minimize (5). Conversely, we can assume these descriptors as fixed (fulfilling the concept of conservation of morphological description mentioned before) and introduce a realization of a dense deformation field $U: \mathbb{R}^n \to \mathbb{R}^n$ that maps the initial partition Ω_0 to the estimated one:

$$\Omega' = \Omega_0 + \hat{U}. \tag{7}$$

Thus, (6) is rewritten as $p(U \mid F) \propto p(F \mid U) p(U)$ that yields the following MAP solution:

$$\hat{U} = \operatorname*{argmax}_{U} \left\{ p(U \mid F) \right\} = \operatorname*{argmax}_{U} \left\{ p(F \mid U) \, p(U) \right\}. \quad (8)$$

An extended assumption is that the feature vector realization F is *i.i.d.*, and thus, it is possible to write the a-posteriori probability $p(F \mid U)$ as a continuous product with $d\mathbf{x}$ the infinitesimal voxel size:

$$p(F \mid U) p(U) = \prod_{l} \prod_{\mathbf{x} \in \Omega'_{l}} p_{l} \left(F(\mathbf{x} + U(\mathbf{x})) \mid U(\mathbf{x}) \right)^{d\mathbf{x}}. \quad (9)$$

I'm not convinced about turning $p(\Omega)$ into p(U).

A second widely-accepted assumption is the multivariate normal distribution of the different tissues in MRI data. Therefore, the posterior probability of an infinitesimal voxel can be written as:

$$p_l(F(\mathbf{x}) \mid U(\mathbf{x})) = \frac{1}{\sqrt{(2\pi)^C |\mathbf{\Sigma}_l|}} e^{\left(-\frac{1}{2}\Delta_l^2(\mathbf{f}')\right)}.$$
 (10)

where we can identify the factor in the exponential as the squared *Mahalanobis distance* of the feature observed in the displaced position, $\mathbf{f}' = F(\mathbf{x} + U(\mathbf{x}))$ with region descriptors $\Theta_l = \{\boldsymbol{\mu}_l, \boldsymbol{\Sigma}_l\}$:

$$\Delta_l^2(\mathbf{f} \mid \Theta_l) = (\mathbf{f} - \boldsymbol{\mu}_l)^T \boldsymbol{\Sigma}_l^{-1} (\mathbf{f} - \boldsymbol{\mu}_l).$$
 (11)

Finally, we can turn the MAP problem into a variational one applying the following log-transform:

$$E(F \mid U) = -\log [p(F \mid U) p(U)] =$$

$$= -\log \left[\prod_{l} \prod_{\mathbf{x} \in \Omega'_{l}} p_{l}(F(\mathbf{x}) \mid U(\mathbf{x}))^{d\mathbf{x}} \right] =$$

$$= \sum_{l} \int_{\Omega'_{l}} -\log [p_{l}(F(\mathbf{x}) \mid U(\mathbf{x}))] d\mathbf{x}, \quad (12)$$

and introducing the posterior probability term (10), we can express the functional in terms of the deformation field \boldsymbol{U} and

the region descriptors Θ_l :

$$E(U) =$$

$$= \sum_{l} \int_{\Omega'_{l}} -\log \left[\frac{1}{\sqrt{(2\pi)^{C} |\mathbf{\Sigma}_{l}|}} e^{\left(-\frac{1}{2}\Delta_{l}^{2}(\mathbf{f})\right)} \right] d\mathbf{x} =$$

$$= \sum_{l} \int_{\Omega'_{l}} \left[\frac{1}{2} \log \left((2\pi)^{C} |\mathbf{\Sigma}_{l}| \right) + \frac{1}{2} \Delta_{l}^{2}(\mathbf{f}) \right] d\mathbf{x}. \quad (13)$$

Finally, after removing scaling factors and independent constants, we obtain:

$$E(U) = \sum_{l} \left[|\Omega'_{l}| \log |\mathbf{\Sigma}_{l}| + \int_{\Omega'_{l}} \Delta_{l}^{2}(\mathbf{f}) d\mathbf{x} \right], \quad (14)$$

where we have a constant term scaled by the total volume of the partition Ω_l and the determinant of the covariance matrix of the partition $|\Sigma_l|$, plus an energy term based on the squared *Mahalanobis distance*. As long as this shape-based registration framework is designed to allow small changes between boundaries (and therefore, their volumes), and the shape descriptors should not change significantly due to the conservation principle, the first term can be optionally dismissed with respect the second one, what yields:

$$E(U) = \sum_{l} \int_{\Omega_{l}^{\prime}} \Delta_{l}^{2}(\mathbf{f}) d\mathbf{x}.$$
 (15)

This latter expression resembles the Mumford-Shah functional [61] which is at the background of all ACWE-based methods. In this case, (15) includes covariance as region descriptor, what modifies the original functional in a way that it can deal with more general distributions. This is necessary to avoid the assumption that regions Ω_l have a fixed covariance matrix on their complete domain. One immediate advantage of this functional from the original one is the possibility to distinguish regions with the same mean vector but different covariance matrix [72]. In this work, the Mumford-Shah functional is derived for this extension as follows:

$$E(\Theta_{l}, \Omega_{l}) = \sum_{l} \int_{\Omega_{l}} \left[\log |\mathbf{\Sigma}_{l}| + \Delta_{l}^{2}(\mathbf{f}) \right] d\mathbf{x}$$
$$+ \lambda \int_{\Omega_{l} - d\Omega_{l}} (|\nabla \mu|^{2} + |\nabla \mathbf{\Sigma}_{l}|^{2}) d\mathbf{x} + \nu |d\Omega_{l}|, \quad (16)$$

that is easily identifiable with (14) when we apply the so-called *cartoon limit*, for $\lambda \to \infty$:

$$E(\Theta_l, d\Omega_l) = \sum_{l} \int_{\Omega_l} \left[\log |\mathbf{\Sigma}_l| + \Delta_l^2(\mathbf{f}) \right] d\mathbf{x} + \nu |d\Omega_l|.$$
 (17)

As long as we do not penalize the edge set $d\Omega_l$ length, $\nu=0$ and the result is dual to (14):

$$E(\Theta_l, d\Omega_l) = \sum_{l} \int_{\Omega_l} \left[\log |\mathbf{\Sigma}_l| + \Delta_l^2(\mathbf{f}) \right] d\mathbf{x}.$$
 (18)

C. Introducing priors

By introducing U in (6), we transformed the segmentation problem into a registration one provided with Ω_0 (the initial partition) is derived from the shape-priors given in reference

space. Therefore, the priors can be expressed in terms of the deformation field:

$$P(U) = \prod_{\mathbf{x}} p(U(\mathbf{x}))^{d\mathbf{x}}.$$
 (19)

We define $P(U(\mathbf{x})) = p(\mathbf{u}) = \prod_d p_d(\mathbf{u})$ with d the order of the derivative. We also assume that an initial affine registration let us consider that the deformation field (d=0) and its derivatives up to some order (d>0) are all zero mean, and have some variance Σ_d . We restrict ourselves to $d=\{0,1\}$ (the field and its gradient):

$$p_0(\mathbf{u}) = \mathcal{N}(\mathbf{u} \mid 0, \alpha^{-1}), \tag{20a}$$

$$p_1(\mathbf{u}) = \mathcal{N}(\nabla \mathbf{u} \mid 0, \Sigma_{\beta}^{-1}),$$
 (20b)

And therefore:

$$P(U) = \prod_{\mathbf{x}} \left[p_0(\mathbf{u}) \, p_1(\mathbf{u}) \right]^{d\mathbf{x}}. \tag{21}$$

D. Numerical Implementation

Let us denote $\{c_i\}_{i=1...N_c}$ the nodes of one or several shape-prior surface(s). In our application, precise tissue interfaces of interest extracted from a high-resolution, anatomically correct reference volume. On the other hand, we have a number of dMRI-derived features at each voxel of the volume. Let us denote by \mathbf{x} the voxel and $f(\mathbf{x}) = [f_1, f_2, \ldots, f_N]^T(\mathbf{x})$ its associated feature vector.

1) Deformation field: The transformation from reference into dMRI coordinate space is achieved through a dense deformation field $u(\mathbf{x})$, such that:

$$c'_{i} = T\{c_{i}\} = c_{i} + u(c_{i}),$$
 (22)

what is equivalent to (7). Since the nodes of the anatomical surfaces might lay off-grid, it is required to derive $u(\mathbf{x})$ from a discrete set of parameters $\{u_k\}_{k=1...K}$. Densification is achieved through a set of associated basis functions ψ_k (e.g. rbf, interpolation splines):

$$u(\mathbf{x}) = \sum_{k} \psi_k(\mathbf{x}) u_k \tag{23}$$

In our implementation, ψ_k is chosen to be a tensor-product B-Spline kernel. Then, the transformation writes

$$c'_{i} = T\{c_{i}\} = c_{i} + u(c_{i}) = c_{i} + \sum_{k} \psi_{k}(c_{i}) u_{k}$$
 (24)

Based on the current estimate of the distortion u, we can compute "expected samples" within the shape prior projected into the dMRI. Thus, we now estimate region descriptors of the dMRI features $f(\mathbf{x})$ of the regions defined by the priors in dMRI space. Using the region descriptors derived in subsection II-B, we propose an ACWE-like, piece-wise constant, variational image segmentation model (where the unknown is the deformation field) [73] with the energy functional obtained in (15). This inverse problem is ill-posed [74, 75]. In order to account for deformation field regularity and to render the

problem well-posed, we include limiting and regularization terms into the energy functional [76, 77]:

$$E(u) = \sum_{l} \int_{\Omega'_{l}} \Delta_{l}^{2}(\mathbf{f}) d\mathbf{x}$$
$$+ \int u^{T} A u d\mathbf{x} + \int \operatorname{tr}\{(\nabla u^{T})^{T} B(\nabla u^{T})\} d\mathbf{x} \quad (25)$$

These regularity terms ensure that the segmenting contours in dMRI space are still close to their native shape. The model easily allows to incorporate inhomogeneous and anisotropic regularization [78] to better regularize the EPI distortion.

2) Operator splitting: In order to make the energy minimization computationally more tractable, we propose the following operator splitting: Let us optimize the data terms and the regularity terms on separate copies of the deformation field, now called u and v, constrained to be equal:

$$E(u, v) = \sum_{l} \int_{\Omega'_{l}(u)} \Delta_{l}^{2}(\mathbf{f}) d\mathbf{x}$$
$$+ \int v^{T} A v d\mathbf{x} + \int \operatorname{tr}\{(\nabla v^{T})^{T} B(\nabla v^{T})\} d\mathbf{x} \quad (26)$$

and now

$$\min_{u,v} \{E\} \quad s.t. \quad u = v. \tag{27}$$

In order to take the equality constraint into account, we may make use of augmented Lagrangians (a combination of Lagrangian multipliers and penalty terms on the constraint) [79–81]:

$$AL(u, v, \lambda, r) = E(u, v) + \langle \lambda, u - v \rangle + \frac{r}{2} \|u - v\|_2^2$$
 (28)

To solve the constraint minimization problem, we may now optimize the Augmented Lagrangian in an iterative way:

$$\begin{cases} u^{t+1} &= \operatorname{argmin}_{u} AL(u, v^{t}, \lambda^{t}, r) \\ v^{t+1} &= \operatorname{argmin}_{v} AL(u^{t+1}, v, \lambda^{t}, r) \\ \lambda^{t+1} &= \lambda^{t} + \rho(u^{t+1} - v^{t+1}) \end{cases}$$
 (29)

where typically $0 < \rho < r$. The two sub-minimization problems will now be much easier to handle than the original complete problem.

3) Shape gradients: To compute the gradient-descent of the data-term domain integrals with respect to the underlying deformation field, we use shape gradients [70, 71]. A little bit of theory is therefore in order.

Let Ω be an image domain and $d\Omega$ its boundary. Further, $r(\mathbf{x})$ is an "arbitrary" function over the image domain. We now derive the domain integral w.r.t. the contour evolution parameter t (time):

$$\frac{\partial}{\partial t} \int_{\Omega} r(\mathbf{x}) d\mathbf{x} = \int_{\Omega} \frac{\partial r}{\partial t}(\mathbf{x}) d\mathbf{x} - \int_{d\Omega} r(\mathbf{x}) \left\langle \frac{\partial d\Omega}{\partial t}, N_{d\Omega} \right\rangle d\mathbf{x}$$
(30)

where $\langle \frac{\partial d\Omega}{\partial t}, N_{d\Omega} \rangle$ is the projection of the boundary movement on the unit inward normal. We recall here that equation (30) stands the bridge between the explicit level set formulations surveyed in subsection II-A with the presented approach in setting up the velocity function.

4) Minimization w.r.t. u: The first minimization problem optimizes the data-term. The problem is equivalent to minimizing the following energy:

$$E(u,v) = \sum_{l} \int_{\Omega'_{l}(u)} \Delta_{l}^{2}(\mathbf{f}) d\mathbf{x} + \langle \lambda, u - v \rangle + \frac{r}{2} \|u - v\|_{2}^{2}$$
(31)

where we identify one instance of domain integrals of the form $\int_{\Omega} r(\mathbf{x}) d\mathbf{x}$ for each region l. Optimality requires the derivative of this energy with respect to the parameters u to be null. At this point, we decide to ignore the influence of the boundary shift on the statistics of the regions (i.e. moving the boundary does not significantly impact the μ and Σ descriptors). This means that we can drop the derivative of $r(\mathbf{x})$ w.r.t. contour evolution. What remains are the surface integrals at the subdomain interfaces, plus the Lagrangian and penalty terms:

$$\frac{\partial E}{\partial u_k} = \sum_{l} \int_{d\Omega'_l} \left[\Delta_{O(l)}^2(\mathbf{f}) - \Delta_l^2(\mathbf{f}) \right] \left\langle \frac{\partial d\Omega'_l}{\partial t}, N_{d\Omega'_l} \right\rangle d\mathbf{x} + \lambda_k + r(u_k - v_k) = 0 \quad (32)$$

where O(l) is a function that returns the neighboring region at \mathbf{x} (i.e. the region *outside* the current location in the contour). For the shake of simple notation, we will refer as c' to the positions of points belonging to any of the existing contours $d\Omega_l$. Given the deformation field interpolation stated in subsubsection II-D1, the boundary moves according to

$$\frac{\partial c'}{\partial u_k} = \psi_k(c') \, e_a \tag{33}$$

where e_a is the unit vector along direction $a \in \mathbb{R}^n$ and n the dimension of the image. Thus

$$\left\langle \frac{\partial c'}{\partial u_k}, N_{c'} \right\rangle = \psi_k(c') \,\hat{\mathbf{n}}_{c'}$$
 (34)

The discrete implementation of (32) is straightforward as we have a triangularized mesh representation of the interfacing surfaces:

$$\frac{\partial E}{\partial u_k} = \sum_{l} \sum_{c'} \left[\Delta_{O(l)}^2(\mathbf{f}) - \Delta_l^2(\mathbf{f}) \right] \psi_l(c') \,\hat{\mathbf{n}}_{c'} + \lambda_k + r(u_k - v_k) = 0 \quad (35)$$

The optimal distortion u_k is found at each iteration as:

$$u_k^{t+1} = v_k^t - \frac{1}{r} \lambda_k^t$$
$$- \frac{1}{r} \sum_{l} \sum_{c'} \left[\Delta_{O(l)}^2(\mathbf{f}) - \Delta_l^2(\mathbf{f}) \right] \psi_k(c') \,\hat{\mathbf{n}}_{c'} \quad (36)$$

5) Minimization w.r.t. v: For the optimization w.r.t. v, the relevant energy writes

$$E(v) = \int v^T A v d\mathbf{x} + \int \operatorname{tr}\{(\nabla v^T)^T B(\nabla v^T)\} d\mathbf{x}$$
 (37)

$$+ \langle \lambda, u - v \rangle + \frac{r}{2} \|u - v\|_2^2$$

Do not assume this

Let's assume the simplest, homogeneous isotropic case, $A=\alpha/2$ and $B=\beta/2$. The associated Euler-Lagrange equation is found as:

$$\alpha v - \beta \Delta v + rv = ru + \lambda \tag{38}$$

which easily translates into Fourier domain:

$$v^{t+1} = \mathcal{F}^{-1} \left\{ \frac{\mathcal{F}\{ru + \lambda\}}{\mathcal{F}\{(\alpha + r)\mathcal{I} - \beta\Delta\}} \right\}$$
 (39)

where \mathcal{I} denotes the identity operator.

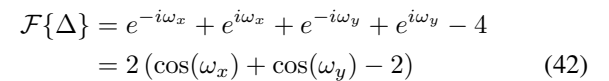
Here, we rewrite the Laplacian as a linear combination of the identity and shift operators:

$$\Delta = \sum_{d} \mathcal{S}_{d}^{-} + \mathcal{S}_{d}^{+} - 2\mathcal{I} \tag{40}$$

where S_d^{\pm} stands for the forward (+) and backward (-) shift operator along coordinates axis d, of which the Fourier transform is found easily as

$$\mathcal{F}\{\mathcal{S}_d^{\pm}\} = e^{\pm i\omega_d},\tag{41}$$

where ω_d is the normalized pulsation along d-direction. Accordingly, the Fourier transform of the discrete Laplacian is found as



The remaining transforms are trivial or can be computed using FFT (as in [82]).

6) Lagrangian multiplier update: At each iteration, the Lagrangian multipliers are updated as noted before:

$$\lambda^{t+1} = \lambda^t + \rho(u^{t+1} - v^{t+1}) \tag{43}$$

- 7) Region descriptor reestimation: In regular intervals, i.e. after n iterations, the parameters μ and Σ of the involved regions need to be reestimated based on the shifted volumetric samples w_j' , g_j' and o_j' .
- 8) Convergence: In order to "fixate" the evolution when close to convergence, it is advised to slightly increase the penalty weight r at each iteration. Note that as can be seen in the above equations, r governs the step-size or leash-length at each iteration, i.e. the amount by which the new estimate u may move away from the preceding v and vice-versa.

III. DATA AND EXPERIMENTS

A. Image Data

1) Simulated digital phantom: The lack of a widely accepted gold-standard in the application field has been addressed by several authors [83] In this work, we use one of the most complete, and publicly available, digital phantoms (http://hardi.epfl.ch/static/events/2013_ISBI/testing_data.html). The phantom is a spherical volume containing a set of fiber bundles, that connect one area of a "cortex" to another. The model accounts for PVE using a similar approach to [84] and for CSF contamination as well.

2) Real MRI datasets: We used image data from XX healthy volunteers with no history of neurological conditions (ages XX±XX, X female) to illustrate the applicability of our approach. All the subjects were scanned in a 3T MR Scanner (Siemens Magnetom TrioTim, Siemens, Erlangen, Germany) with a standard 12-channel head coil.

check coil # channels

Subjects were scanned twice with the same protocol, described hereafter. After being scanned the first time, each subject exited the scan room for a short break and then reentered for an identical scan session. To note, there was a full repositioning of the volunteer, coils, blankets and pads before each scan and re-scan session. The scan session protocol was as follows:

- 1) Triplanar survey (Localizer).
- Field Mapping: field mapping using GRE sequence was performed before dMRI acquisition for susceptibility correction purposes.
- 3) DTI: dMRI were acquired with axial in-plane isotropic resolution 2mm, slice thickness 2mm, $XXX \times XXX \times XX$
- 4) Field Mapping (same as before DTI)
- 5) Structural T1: An MPRAGE T1-weighted acquisition, sagittal GRE sequence, in-plane isotropic resolution 1.0 mm, slice thickness 1.2mm $XXX \times XXX \times XXX$ image matrix, TR=2300 ms, TE=2.98 ms, FA= 9, NEX=X, BW= 240 Hz/pixel.
- 6) Structural T2: A T2-weighted acquisition, oblique axial TSE sequence, in-plane isotropic resolution 1.0 mm, slice thickness 1.2mm $XXX \times XXX \times XXX$ image matrix, TR=3200 ms, TE= 408 ms, NEX=X, BW= 751 Hz/pixel.

B. Image preprocessing and shape-prior generation

Regardless the dataset type (simulated or real), all dMRI datasets were processed using the standard diffusion tensor imaging (DTI) reconstruction methods provided by FSL ¹ to fit the tensor model and produce scalar maps of the required features. The properties of the reconstructed tensors and derived scalar maps have been studied by [20]. Based on their findings, FA (44) and MD (45) are considered complementary features, and therefore we selected them for the energy model (25) in driving the registration-segmentation process. Whereas FA informs mainly about the *shape* of diffusion, the MD is more related to the *magnitude* of the process:

$$FA = \sqrt{\frac{1}{2}} \frac{\sqrt{(\lambda_1 - \lambda_2)^2 + (\lambda_2 - \lambda_3)^2 + (\lambda_3 - \lambda_1)^2}}{\sqrt{\lambda_1^2 + \lambda_2^2 + \lambda_3^2}}$$
(44)

$$MD = (\lambda_1 + \lambda_2 + \lambda_3)/3 \tag{45}$$

where λ_i are the eigenvalues of the diffusion tensor associated with the diffusion signal $S(\vec{q})$. There exist two main reasons to justify their choice. First, they are well-understood and standardized in clinical routine. Second, together they contain most of the information that is usually extracted from the dMRI-derived scalar maps [20].

Preprocessing differed between simulated and real datasets in the shape-prior surfaces generation, as we describe hereafter

- 1) Simulated digital phantom: A description goes here: surfaces extraction, synthetic susceptibility artifact generation.
- 2) Real MRI data: We used a standard automated method available in FreeSurfer [48] to obtain the cortical gray/white boundary from the T1 scan [46]. Parcellations used to evaluate the repeatability of the method are also obtained from FreeSurfer.

C. Experiments and evaluation

- 1) Validation on the simulated digital phantom: We firstly evaluated our approach on the simulated data, using the distorted data with a deformation field similar to the susceptibility artifact that affects real dMRI data. To this end, we report the following indices:
 - Surface error (SE), a distance between the one-to-one corresponding vertices, weighted by their respective Voronoi area

$$MSE = \sum_{k} \sum_{j}^{M} w_j \|\mathbf{x}_j - \hat{\mathbf{x}}_j\|$$
 (46)

where \mathbf{x}_j are the locations of the M vertices of the k priors, $\hat{\mathbf{x}}_j$ are the corresponding locations recovered, and w_j the weighting factor as the relative surface of the Voronoi area.

 Warping index (WI), L2-distance between the theoretical and the recovered deformation field.

$$WI = \frac{1}{N} \sum_{i}^{N} \|\mathbf{d}_{i} - \hat{\mathbf{d}}_{i}\| \tag{47}$$

where \mathbf{d}_i is the theoretical displacement vector at position i and $\hat{\mathbf{d}}_i$ is the recovered one at the same index position.

- Parcellation agreement, the SE averaged by defined region of interests (ROIs) between the theoretical and the recovered parcellations.
- number of fibers (NoF) agreement, between the fibers recovered on the original data and the processed data.

Additionally, the entropy of data is studied in both original and recovered datasets to draw another possible basis for the assessment of the real datasets. We also report the same indices for the outcome of a widely-used methodology that combines field-map susceptibility correction and T1-T2-dMRI registration .

¹DTIFIT, included in the FMRIB's Software Library (FSL), http://fsl.fmrib.ox.ac.uk/fsl/fsl-4.1.9/fdt/fdt_dtifit.html

I suggest to give it a compact name and define it in the pre-processing section or even before in the intro

2) Evaluation on real datasets: For the real datasets there is no published *gold*-standard to validate results. Thus, visual results are provided to let compare the performance with the NICEACRONYM standard methodology. Additionally, cross-comparison of repeatability results are provided. In this second evaluation strategy, all the indices defined in subsubsection III-C1 are reported.

IV. RESULTS AND DISCUSSION

Please! Write me ASAP.

V. CONCLUSION

A novel application for the ACWE framework is proposed, with the aim at recovering the displacement field underlying the EPI geometrical distortions. Exploiting the segmentation properties of the ACWE and optimizing the displacement field, we describe a registration-segmentation methodology that simultaneously segmented and restored the distortion on dMRI-like synthetic data. Visual results and quantitative results are provided.

We implemented the methodology upon the widely used Insight Registration and Segmentation Toolkit ² (ITK) for its computational benefits, the standardized code, and with the aim at making the procedure publicly available when ready for sharing with the research community.

Once proven the aptness of the methodology to the application with simplistic synthetic data, in further studies we will cover the actual performance on real images and the benefits of overcoming the described challenges (segmentation and EPI distortion correction) in one single step. Additional research lines regard with the use of more adequate optimization schemes and the use of an energy model better adapted to the specific nature of the dMRI data.

We conclude recalling the importance of tackling with the numerous challenges that exist on the dMRI data processing in order to achieve reliable results on the whole-brain connectivity analysis.

ACKNOWLEDGMENT

The authors gratefully acknowledge V. Estellers for critical discussions at early stages of this project, A. Griffa for acquiring the real datasets used in this work, K. O'Brien for his discussions and clarifications regarding distortions and their foundations in dMRI, E. Caruyer for providing us with the simulated digital phantom, and L. Vese for her generous support.

REFERENCES

[1] P. C. Sundgren, Q. Dong, D. Gómez-Hassan, S. K. Mukherji, P. Maly, and R. Welsh, "Diffusion tensor imaging of the brain: review of clinical applications," *Neuroradiology*, vol. 46,

²http://www.itk.org

- pp. 339–350, May 2004. [Online]. Available: http://www.springerlink.com/content/fa30k4q3h9kg4yjq/
- [2] R. C. Craddock, S. Jbabdi, C.-G. Yan, J. T. Vogelstein, F. X. Castellanos, A. Di Martino, C. Kelly, K. Heberlein, S. Colcombe, and M. P. Milham, "Imaging human connectomes at the macroscale," *Nature Methods*, vol. 10, no. 6, pp. 524–539, Jun. 2013. [Online]. Available: http://www.nature.com/nmeth/journal/v10/n6/abs/nmeth.2482.html
- [3] P. J. Basser and C. Pierpaoli, "Microstructural and physiological features of tissues elucidated by quantitative-diffusion-tensor MRI," *Journal of Magnetic Resonance*, vol. 213, no. 2, pp. 560–570, Dec. 2011. [Online]. Available: http://www.sciencedirect.com/science/article/pii/S109078071100334X
- [4] P. Hagmann, P. E. Grant, and D. A. Fair, "MR connectomics: a conceptual framework for studying the developing brain," Frontiers in Systems Neuroscience, vol. 6, Jun. 2012, PMID: 22707934 PMCID: PMC3374479. [Online]. Available: http://www.ncbi.nlm.nih.gov/pmc/articles/PMC3374479/
- [5] H. Johansen-Berg and M. F. Rushworth, "Using diffusion imaging to study human connectional anatomy," *Annual Review of Neuroscience*, vol. 32, no. 1, pp. 75–94, 2009, PMID: 19400718. [Online]. Available: http://www.annualreviews.org/doi/ abs/10.1146/annurev.neuro.051508.135735
- [6] P. Hagmann, "From diffusion MRI to brain connectomics," Ph.D. dissertation, Institut de traitement des signaux PROGRAMME DOCTORAL EN INFORMATIQUE ET COMMUNICATIONS POUR L'OBTENTION DU GRADE DE DOCTEUR ÈS SCIENCES PAR Docteur en médecine, Université de Lausanne, 2005. [Online]. Available: http://biblion.epfl. ch/EPFL/theses/2005/3230/EPFL_TH3230.pdf
- [7] O. Sporns, G. Tononi, and R. Kötter, "The human connectome: A structural description of the human brain," *PLoS computational biology*, vol. 1, no. 4, p. e42, Sep. 2005, PMID: 16201007.
- [8] J. L. Morgan and J. W. Lichtman, "Why not connectomics?" *Nature Methods*, vol. 10, no. 6, pp. 494–500, Jun. 2013. [Online]. Available: http://www. nature.com/nmeth/journal/v10/n6/full/nmeth.2480.html
- [9] A. Griffa, P. S. Baumann, J.-P. Thiran, and P. Hagmann, "Structural connectomics in brain diseases," *NeuroImage*, vol. In press, 2013. [Online]. Available: http://www.sciencedirect.com/science/article/ pii/S1053811913004035
- [10] A. Daducci, S. Gerhard, A. Griffa, A. Lemkaddem, L. Cammoun, X. Gigandet, R. Meuli, P. Hagmann, and J.-P. Thiran, "The connectome mapper: An opensource processing pipeline to map connectomes with MRI," *PLoS ONE*, vol. 7, no. 12, p. e48121, Dec. 2012. [Online]. Available: http://dx.doi.org/10.1371/ journal.pone.0048121
- [11] E. Bullmore and O. Sporns, "Complex brain networks: graph theoretical analysis of structural and functional systems," *Nature Reviews Neuroscience*, vol. 10, no. 3,

- pp. 186–198, Mar. 2009. [Online]. Available: http://www.nature.com/nrn/journal/v10/n3/abs/nrn2575.html
- [12] D. E. Meskaldji, E. Fischi-Gomez, A. Griffa, P. Hagmann, S. Morgenthaler, and J.-P. Thiran, "Comparing connectomes across subjects and populations at different scales," *NeuroImage*, vol. In Press, 2013. [Online]. Available: http://www.sciencedirect.com/science/article/pii/S105381191300431X
- [13] D. K. Jones and M. Cercignani, "Twenty-five pitfalls in the analysis of diffusion MRI data," *NMR in Biomedicine*, vol. 23, no. 7, p. 803–820, 2010. [Online]. Available: http://onlinelibrary.wiley.com/doi/ 10.1002/nbm.1543/abstract
- [14] H. Cheng, Y. Wang, J. Sheng, W. G. Kronenberger, V. P. Mathews, T. A. Hummer, and A. J. Saykin, "Characteristics and variability of structural networks derived from diffusion tensor imaging," *NeuroImage*, vol. 61, no. 4, pp. 1153–1164, Jul. 2012. [Online]. Available: http://www.sciencedirect.com/science/article/ pii/S1053811912003175
- [15] D. K. Jones, T. R. Knösche, and R. Turner, "White matter integrity, fiber count, and other fallacies: The do's and don'ts of diffusion MRI," *NeuroImage*, vol. 73, pp. 239–254, Jun. 2013. [Online]. Available: http://www.sciencedirect.com/science/article/ pii/S1053811912007306
- [16] P. Mukherjee, S. W. Chung, J. I. Berman, C. P. Hess, and R. G. Henry, "Diffusion tensor MR imaging and fiber tractography: Technical considerations," *American Journal of Neuroradiology*, vol. 29, no. 5, pp. 843–852, May 2008, PMID: 18339719. [Online]. Available: http://www.ajnr.org/content/29/5/843
- [17] J. M. Soares, P. Marques, V. Alves, and N. Sousa, "A hitchhiker's guide to diffusion tensor imaging," *Frontiers in Brain Imaging Methods*, vol. 7, p. 31, 2013. [Online]. Available: http://www.frontiersin.org/Brain_Imaging_Methods/10.3389/fnins.2013.00031/abstract
- [18] K. O'Brien, A. Daducci, N. Kickler, F. Lazeyras, R. Gruetter, T. Feiweier, and G. Krueger, "3D residual eddy current field characterisation: applied to diffusion weighted magnetic resonance imaging," *IEEE Transac*tions on Medical Imaging, vol. Early Access Online, 2013
- [19] A. Daducci, "ISBI2013 dMRI reconstruction challenge," *IEEE Transactions on Medical Imaging*, vol. ??, no. ??, 2013, REPLACE THIS REF when it is published.
- [20] D. B. Ennis and G. Kindlmann, "Orthogonal tensor invariants and the analysis of diffusion tensor magnetic resonance images," *Magnetic Resonance* in *Medicine*, vol. 55, no. 1, p. 136–146, 2006. [Online]. Available: http://onlinelibrary.wiley.com/doi/ 10.1002/mrm.20741/abstract
- [21] A. L. Alexander, K. M. Hasan, M. Lazar, J. S. Tsuruda, and D. L. Parker, "Analysis of partial volume effects in diffusion-tensor MRI," *Magnetic resonance in medicine: official journal of the Society of Magnetic Resonance in Medicine / Society of Magnetic Resonance in Medicine*, vol. 45, no. 5, pp. 770–780, May 2001, PMID: 11323803.

- [22] C. Metzler-Baddeley, M. J. O'Sullivan, S. Bells, O. Pasternak, and D. K. Jones, "How and how not to correct for CSF-contamination in diffusion MRI," *NeuroImage*, vol. 59, no. 2, pp. 1394–1403, Jan. 2012. [Online]. Available: http://www.sciencedirect.com/ science/article/pii/S1053811911009426
- [23] S. Jbabdi and H. Johansen-Berg, "Tractography: Where do we go from here?" *Brain Connectivity*, vol. 1, no. 3, pp. 169–183, 2011. [Online]. Available: http://online.liebertpub.com/doi/abs/10.1089/brain.2011.0033
- [24] L. Zhukov, K. Museth, D. Breen, R. Whitaker, and A. Barr, "Level set modeling and segmentation of DT-MRI brain data," *Journal of Electronic Imaging*, vol. 12, no. 1, p. 125–133, 2003.
- [25] M. Rousson, C. Lenglet, and R. Deriche, "Level set and region based surface propagation for diffusion tensor MRI segmentation," in *Computer Vision and Mathematical Methods in Medical and Biomedical Image Analysis*, ser. Lecture Notes in Computer Science. Springer Berlin Heidelberg, Jan. 2004, no. 3117, pp. 123–134. [Online]. Available: http://link.springer.com/chapter/10.1007/978-3-540-27816-0_11
- [26] L. Jonasson, X. Bresson, J. Thiran, V. Wedeen, and P. Hagmann, "Representing diffusion MRI in 5-d simplifies regularization and segmentation of white matter tracts," *IEEE Transactions on Medical Imaging*, vol. 26, no. 11, pp. 1547–1554, 2007.
- [27] A. Hadjiprocopis, W. Rashid, and P. S. Tofts, "Unbiased segmentation of diffusion-weighted magnetic resonance images of the brain using iterative clustering," *Magnetic Resonance Imaging*, vol. 23, no. 8, pp. 877–885, Oct. 2005. [Online]. Available: http://www.sciencedirect.com/science/article/pii/S0730725X05002304
- [28] T. Liu, H. Li, K. Wong, A. Tarokh, L. Guo, and S. T. Wong, "Brain tissue segmentation based on DTI data," *NeuroImage*, vol. 38, no. 1, pp. 114–123, Oct. 2007. [Online]. Available: http://www.sciencedirect.com/ science/article/pii/S1053811907005873
- [29] S. Awate, H. Zhang, T. Simon, and J. Gee, "Multivariate segmentation of brain tissues by fusion of MRI and DTI data," in 5th IEEE International Symposium on Biomedical Imaging: From Nano to Macro, 2008. ISBI 2008, 2008, pp. 213–216.
- [30] C.-F. Lu, P.-S. Wang, Y.-C. Chou, H.-C. Li, B.-W. Soong, and Y.-T. Wu, "Segmentation of diffusion-weighted brain images using expectation maximization algorithm initialized by hierarchical clustering," in 30th Annual International Conference of the IEEE Engineering in Medicine and Biology Society, 2008. EMBS 2008, 2008, pp. 5502–5505.
- [31] D. Han, V. Singh, J. Lee, E. Zakszewski, N. Adluru, T. Oakes, and A. Alexander, "An experimental evaluation of diffusion tensor image segmentation using graph-cuts," in *Engineering in Medicine and Biology Society*, 2009. EMBC 2009. Annual International Conference of the IEEE, 2009, p. 5653–5656.
- [32] S. Kumazawa, T. Yoshiura, H. Honda, F. Toyofuku, and Y. Higashida, "Partial volume estimation and segmen-

- tation of brain tissue based on diffusion tensor MRI," *Medical physics*, vol. 37, no. 4, pp. 1482–1490, Apr. 2010, PMID: 20443469.
- [33] S. Kumazawa, T. Yoshiura, H. Honda, and F. Toyofuku, "Improvement of partial volume segmentation for brain tissue on diffusion tensor images using multiple-tensor estimation," *Journal of Digital Imaging*, pp. 1–10, Apr. 2013. [Online]. Available: http://link.springer.com/article/10.1007/s10278-013-9601-z
- [34] A. K. Jha, M. A. Kupinski, J. J. Rodríguez, R. M. Stephen, and A. T. Stopeck, "Task-based evaluation of segmentation algorithms for diffusion-weighted MRI without using a gold standard," *Physics in Medicine and Biology*, vol. 57, no. 13, p. 4425, Jul. 2012. [Online]. Available: http://iopscience.iop.org/0031-9155/57/13/4425
- [35] P. Jezzard, A. S. Barnett, and C. Pierpaoli, "Characterization of and correction for eddy current artifacts in echo planar diffusion imaging," *Magnetic resonance in medicine*, vol. 39, no. 5, p. 801–812, 2005. [Online]. Available: http://onlinelibrary.wiley.com/doi/10.1002/mrm.1910390518/abstract
- [36] Y.-C. Hsu, C.-H. Hsu, and W.-Y. Tseng, "Correction for susceptibility-induced distortion in echo-planar imaging using field maps and model-based point spread function," *IEEE Transactions on Medical Imaging*, vol. 28, no. 11, pp. 1850 –1857, Nov. 2009.
- [37] P. J. Reber, E. C. Wong, R. B. Buxton, and L. R. Frank, "Correction of off resonance-related distortion in echo-planar imaging using EPI-based field maps," *Magnetic Resonance in Medicine*, vol. 39, no. 2, p. 328–330, 2005. [Online]. Available: http://onlinelibrary.wiley.com/doi/10.1002/mrm.1910390223/abstract
- [38] J. L. Andersson, C. Hutton, J. Ashburner, R. Turner, and K. Friston, "Modeling geometric deformations in EPI time series," *NeuroImage*, vol. 13, no. 5, pp. 903–919, May 2001. [Online]. Available: http://www.sciencedirect. com/science/article/pii/S1053811901907463
- [39] J. Kybic, P. Thevenaz, A. Nirkko, and M. Unser, "Unwarping of unidirectionally distorted EPI images," *IEEE Transactions on Medical Imaging*, vol. 19, no. 2, pp. 80–93, Feb. 2000.
- [40] C. Studholme, R. Constable, and J. Duncan, "Accurate alignment of functional EPI data to anatomical MRI using a physics-based distortion model," *IEEE Transactions on Medical Imaging*, vol. 19, no. 11, pp. 1115–1127, 2000.
- [41] Y. Li, N. Xu, J. Fitzpatrick, V. Morgan, D. Pickens, and B. Dawant, "Accounting for signal loss due to dephasing in the correction of distortions in gradient-echo EPI via nonrigid registration," *IEEE Transactions on Medical Imaging*, vol. 26, no. 12, pp. 1698–1707, 2007.
- [42] R. Tao, P. T. Fletcher, S. Gerber, and R. T. Whitaker, "A variational image-based approach to the correction of susceptibility artifacts in the alignment of diffusion weighted and structural MRI," in *Information Processing* in *Medical Imaging*, ser. Lecture Notes in Computer Science, J. L. Prince, D. L. Pham, and K. J. Myers, Eds.

- Springer Berlin Heidelberg, Jan. 2009, no. 5636, pp. 664–675. [Online]. Available: http://link.springer.com/chapter/10.1007/978-3-642-02498-6_55
- [43] J. L. Andersson, S. Skare, and J. Ashburner, "How to correct susceptibility distortions in spin-echo echoplanar images: application to diffusion tensor imaging," *NeuroImage*, vol. 20, no. 2, pp. 870–888, Oct. 2003. [Online]. Available: http://www.sciencedirect.com/ science/article/pii/S1053811903003367
- [44] D. Holland, J. M. Kuperman, and A. M. Dale, "Efficient correction of inhomogeneous static magnetic fieldinduced distortion in echo planar imaging," *NeuroImage*, vol. 50, no. 1, p. 175, Mar. 2010, PMID: 19944768 PMCID: PMC2819607. [Online]. Available: http://www. ncbi.nlm.nih.gov/pmc/articles/PMC2819607/
- [45] M. Wu, L.-C. Chang, L. Walker, H. Lemaitre, A. S. Barnett, S. Marenco, and C. Pierpaoli, "Comparison of EPI distortion correction methods in diffusion tensor MRI using a novel framework," in *Medical Image Computing and Computer-Assisted Intervention MICCAI 2008*, ser. Lecture Notes in Computer Science, D. Metaxas, L. Axel, G. Fichtinger, and G. Székely, Eds. Springer Berlin Heidelberg, Jan. 2008, no. 5242, pp. 321–329. [Online]. Available: http://link.springer.com/chapter/10.1007/978-3-540-85990-1 39
- [46] D. N. Greve and B. Fischl, "Accurate and robust brain image alignment using boundary-based registration," *NeuroImage*, vol. 48, no. 1, pp. 63–72, Oct. 2009, PMID: 19573611.
- [47] L. Zöllei, A. Stevens, K. Huber, S. Kakunoori, and B. Fischl, "Improved tractography alignment using combined volumetric and surface registration," *NeuroImage*, vol. 51, no. 1, pp. 206–213, May 2010. [Online]. Available: http://www.sciencedirect.com/science/article/pii/S1053811910001400
- [48] B. Fischl, "FreeSurfer," NeuroImage, vol. 62, no. 2, pp. 774–781, Aug. 2012. [Online]. Available: http://www.sciencedirect.com/science/article/pii/S1053811912000389
- [49] J. Suri, K. Liu, S. Singh, S. Laxminarayan, X. Zeng, and L. Reden, "Shape recovery algorithms using level sets in 2-d/3-d medical imagery: a state-of-the-art review," *IEEE Transactions on Information Technology in Biomedicine*, vol. 6, no. 1, pp. 8–28, 2002.
- [50] X. Bresson, P. Vandergheynst, and J. P. Thiran, "A variational model for object segmentation using boundary information and shape prior driven by the mumford-shah functional," *International Journal of Computer Vision*, vol. 68, no. 2, p. 145–162, 2006. [Online]. Available: http://www.springerlink.com/index/WU0311444417743P.pdf
- [51] T. Chan and W. Zhu, "Level set based shape prior segmentation," in Computer Vision and Pattern Recognition, 2005. CVPR 2005. IEEE Computer Society Conference on, vol. 2, 2005, p. 1164–1170. [Online]. Available: http://ieeexplore.ieee.org/xpls/abs_ all.jsp?arnumber=1467575
- [52] Y. Chen, H. D. Tagare, S. Thiruvenkadam, F. Huang,

- D. Wilson, K. S. Gopinath, R. W. Briggs, and E. A. Geiser, "Using prior shapes in geometric active contours in a variational framework," *International Journal of Computer Vision*, vol. 50, no. 3, pp. 315–328, Dec. 2002. [Online]. Available: http://link.springer.com/article/10.1023/A%3A1020878408985
- [53] D. Cremers, S. J. Osher, and S. Soatto, "Kernel density estimation and intrinsic alignment for shape priors in level set segmentation," *International Journal of Computer Vision*, vol. 69, no. 3, p. 335–351, May 2006.
- [54] M. Gastaud, M. Barlaud, and G. Aubert, "Combining shape prior and statistical features for active contour segmentation," *IEEE Transactions on Circuits and Systems* for Video Technology, vol. 14, no. 5, p. 726–734, May 2004.
- [55] M. Bertalmio, G. Sapiro, and G. Randall, "Morphing active contours," *IEEE Transactions on Pattern Analysis* and Machine Intelligence, vol. 22, no. 7, pp. 733–737, 2000.
- [56] P. P. Wyatt and J. Noble, "MAP MRF joint segmentation and registration of medical images," *Medical Image Analysis*, vol. 7, no. 4, p. 539–552, Dec. 2003.
- [57] N. Paragios, "A level set approach for shape-driven segmentation and tracking of the left ventricle," *IEEE Transactions on Medical Imaging*, vol. 22, no. 6, p. 773–776, Jun. 2003.
- [58] B. Vemuri and Y. Chen, "Joint image registration and segmentation," in *Geometric Level Set Methods in Imaging, Vision, and Graphics*. New York: Springer-Verlag, 2003, p. 251–269.
- [59] A. Yezzi, L. Zöllei, and T. Kapur, "A variational framework for integrating segmentation and registration through active contours," *Medical Image Analysis*, vol. 7, no. 2, p. 171–185, Jun. 2003.
- [60] M. Droske, W. Ring, and M. Rumpf, "Mumford–Shah based registration: a comparison of a level set and a phase field approach," *Computing and Visualization* in Science, vol. 12, no. 3, pp. 101–114, Mar. 2009. [Online]. Available: http://link.springer.com/article/10. 1007/s00791-008-0084-2
- [61] D. Mumford and J. Shah, "Optimal approximations by piecewise smooth functions and associated variational problems," *Communications on Pure and Applied Mathematics*, vol. 42, no. 5, p. 577–685, 1989. [Online]. Available: http://onlinelibrary.wiley.com/doi/ 10.1002/cpa.3160420503/abstract
- [62] S. Gorthi, V. Duay, N. Houhou, M. Bach Cuadra, U. Schick, M. Becker, A. S. Allal, and J.-P. Thiran, "Segmentation of head and neck lymph node regions for radiotherapy planning using active contour-based atlas registration," *IEEE Journal of Selected Topics in Signal Processing*, vol. 3, no. 1, p. 135–147, 2009.
- [63] S. Gorthi, V. Duay, X. Bresson, M. Bach Cuadra, F. J. Sánchez Castro, C. Pollo, A. S. Allal, and J.-P. Thiran, "Active deformation fields: dense deformation field estimation for atlas-based segmentation using the active contour framework," *Medical Image Analysis*, vol. 15, no. 6, p. 787–800, 2011.

- [64] K. M. Pohl, J. Fisher, J. J. Levitt, M. E. Shenton, R. Kikinis, W. E. L. Grimson, and W. M. Wells, "A unifying approach to registration, segmentation, and intensity correction," in *MICCAI* 2005, ser. Lecture Notes in Computer Science, J. S. Duncan and G. Gerig, Eds., vol. 3749. Berlin, Heidelberg: Springer Berlin Heidelberg, 2005, p. 310–318.
- [65] K. M. Pohl, J. Fisher, W. E. L. Grimson, R. Kikinis, and W. M. Wells, "A bayesian model for joint segmentation and registration." *NeuroImage*, vol. 31, no. 1, p. 228–39, May 2006.
- [66] F. Wang, B. C. Vemuri, and S. J. Eisenschenk, "Joint registration and segmentation of neuroanatomic structures from brain MRI." *Academic radiology*, vol. 13, no. 9, p. 1104–11, Sep. 2006.
- [67] A. Yezzi, L. Zollei, and T. Kapur, "A variational framework for joint segmentation and registration," in *MMBIA* 2001. IEEE Comput. Soc, 2001, p. 44–51.
- [68] G. Unal and G. Slabaugh, "Coupled PDEs for nonrigid registration and segmentation," in *IEEE Computer Society Conference on Computer Vision and Pattern Recognition*, 2005. CVPR 2005, vol. 1, 2005, pp. 168– 175 vol. 1.
- [69] S. Osher and J. A. Sethian, "Fronts propagating with curvature-dependent speed: Algorithms based on hamilton-jacobi formulations," *Journal of Computational Physics*, vol. 79, no. 1, pp. 12–49, Nov. 1988. [Online]. Available: http://www.sciencedirect.com/science/article/ pii/0021999188900022
- [70] S. Jehan-Besson, M. Barlaud, and G. Aubert, "DREAM2S: deformable regions driven by an eulerian accurate minimization method for image and video segmentation," *International Journal of Computer Vision*, vol. 53, no. 1, p. 45–70, Jun. 2003.
- [71] A. Herbulot, S. Jehan-Besson, S. Duffner, M. Barlaud, and G. Aubert, "Segmentation of vectorial image features using shape gradients and information measures," *Journal of Mathematical Imaging and Vision*, vol. 25, no. 3, p. 365–386, Aug. 2006. [Online]. Available: http://www.springerlink.com/content/581247x96784v173/http://www.springerlink.com/index/10.1007/s10851-006-6898-y
- [72] T. Brox and D. Cremers, "On local region models and a statistical interpretation of the piecewise smooth mumford-shah functional," *International Journal of Computer Vision*, vol. 84, no. 2, pp. 184–193, Aug. 2009. [Online]. Available: http://link.springer.com/ article/10.1007/s11263-008-0153-5
- [73] T. F. Chan and L. A. Vese, "Active contours without edges," *IEEE Transactions on Image Processing*, vol. 10, no. 2, p. 266–277, 2001.
- [74] M. Bertero, T. A. Poggio, and V. Torre, "Ill-posed problems in early vision," in *Proceedings of the IEEE*, vol. 76, 1988, p. 869–889.
- [75] J. Hadamard, "Sur les problèmes aux dérivées partielles et leur signification physique," *Princeton University Bulletin*, vol. 13, p. 49–52, 1902.
- [76] V. A. Morozov, "Linear and nonlinear ill-posed prob-

- lems," *Journal of Mathematical Sciences*, vol. II, no. 6, p. 706–736, 1975.
- [77] A. N. Tichonov, "Solution of incorrectly formulated problems and the regularization method," *Soviet Mathematics*, vol. 4, p. 1035–1038, 1963.
- [78] H.-H. Nagel and W. Enkelmann, "An investigation of smoothness constraints for the estimation of displacement vector fields from image sequences," *IEEE Transactions on Pattern Analysis and Machine Intelligence*, vol. PAMI-8, no. 5, p. 565–593, Sep. 1986. [Online]. Available: http://ieeexplore.ieee.org/ lpdocs/epic03/wrapper.htm?arnumber=4767833
- [79] D. P. Bertsekas, "Multiplier methods: A survey," *Automatica*, vol. 12, no. 2, p. 133–145, 1976.
- [80] R. Glowinski and P. Le Tallec, Augmented Lagrangian and operator-splitting methods in nonlinear mechanics. Philadelphia: Society for Industrial and Applied Mathematics (SIAM), 1989.
- [81] J. Nocedal and S. J. Wright, *Numerical optimization*, 2nd ed. Springer, Berlin, 2006.
- [82] V. Estellers, D. Zosso, R. Lai, J.-P. Thiran, S. Osher, and X. Bresson, "An efficient algorithm for level set method preserving distance function," in *IEEE Transactions on Image Processing*, 2011.
- [83] M.-A. Côté, G. Girard, A. Boré, E. Garyfallidis, J.-C. Houde, and M. Descoteaux, "Tractometer: Towards validation of tractography pipelines," *Medical Image Analysis*, 2013. [Online]. Available: http://www.sciencedirect.com/science/article/pii/S1361841513000479
- [84] T. G. Close, J.-D. Tournier, F. Calamante, L. A. Johnston, I. Mareels, and A. Connelly, "A software tool to generate simulated white matter structures for the assessment of fibre-tracking algorithms," *NeuroImage*, vol. 47, no. 4, pp. 1288–1300, Oct. 2009, PMID: 19361565.

Oscar Esteban Biography text here.

PLACE PHOTO HERE